Hindawi Publishing Corporation
Journal of Engineering
Volume 2013, Article ID 549865, 10 pages
http://dx.doi.org/10.1155/2013/549865

Research Article

Modal Analysis of 27 mm Piezo Electric Plate for Small-Scale Underwater Sonar-Based Navigation

M. O. Afolayan, D. S. Yawas, C. O. Folayan, and S. Y. Aku

Mechanical Engineering Department, Ahmadu Bello University, Samaru Zaria 810006, Nigeria

Correspondence should be addressed to M. O. Afolayan; tunde_afolayan@yahoo.com

Received 14 September 2012; Revised 15 January 2013; Accepted 12 February 2013

Academic Editor: Jie Zhou

This work presents progress towards the development of a small-scale, purely sonar-based navigation device for a robotic fish (~394 mm long). Aperture overloading of small (5 mm diameter) ultrasonic transmitters does not allow them to be used effectively inside water. A test on a 27 mm diameter buzzer piezo plate shows promising performance under water at frequencies from 4.5 kHz to 80 kHz. ANSYS-based simulation was therefore used to find modal frequencies at higher frequencies so as to optimize this encouraging result. The simulation process also discovered several antiresonant frequencies such as 38.5 kHz, 54 kHz, and 57.5 kHz. All frequencies above the 8th harmonic (10,589.02 Hz) are out of phase with the input load except a resonance frequency of 42.5 kHz and an antiresonance frequency of 56.5 kHz. Also, the first harmonic (1,648.73 Hz) is the only frequency that gave a nodal deformation.

1. Introduction

Many marine organisms such as dolphin navigate using ultrasonic means. Artificial systems such as autonomous underwater vehicles (AUV) and remotely operated system (ROV) commonly use acoustic means in their navigation, object detections, and avoidance, control, and communication. Underwater modems such as those used by Eustice et al. [1] are often based on acoustic links that transmit at a very low frequency to extremely high frequencies while bearing data in the kilobit. (kb) range as exemplified by Kumagai et al. [2] work. According to Eustice et al. [1], "few techniques exist for reliable three-dimensional position sensing for underwater vehicles. Depth, altitude, heading, and roll/pitch attitude can all be instrumented with high-bandwidth internal sensors." Many AUV are equipped with multiple numbers of dead-reckoning sensors, such as Doppler velocity logs and inertial measurement systems, or magnetic compasses to estimate vehicle position. In contrast, the exact coordinate of the robots remains difficult to instrument and is normally measured acoustically in oceanographic and commercial applications and even in submarines [1, 3, 4]. Other methods used on the surface such as inertia navigation and accumulate error that is further aggravated by water waves and currents [5]. Sonar systems have been very attractive for underwater imagery—being capable of longer range and in a variety of water conditions such as poor visibility and lighting [6–8]. The lower frequencies are even more effective for longer ranges as depicted in Table 1; they decay extremely slowly in water [5]. In robotics, sonar systems are often used for ranging due to their low cost and small size. The signal is sent out continuously or pulsed. The pulsed mode is used for eliminating frequent misreading caused by crosstalk or external sources operating nearby [9].

Safety and reliability are factors universally desired in any system design. Navigation based on acoustic has its own inherent problems also. High-power ultrasonic systems have been known to negatively affect underwater ecosystem [14]. Also very powerful low-frequency and activated sonars (and midfrequency sonar) have been claimed to also affect marine life [15].

Another problem is that acoustic degrades in cluttered environments such as reefs or close to the seafloor and subsea structures [8]. In the presence of air bubbles, the signature of object to be detected is adversely affected [16] although algorithms exist for overcoming such limitation.

Table 1: Sonar frequency and its range.

Frequency (kHz)	Range (m)
Low frequency (LF) 8–16	>10000
Medium frequency (MF) 18–36	2000–3000
High frequency (HF) 30–60	1500
Extra high frequency (EHF) 50–110	<1000
Very high frequency (VHF) 200–300	<100

Sources: [10–13].

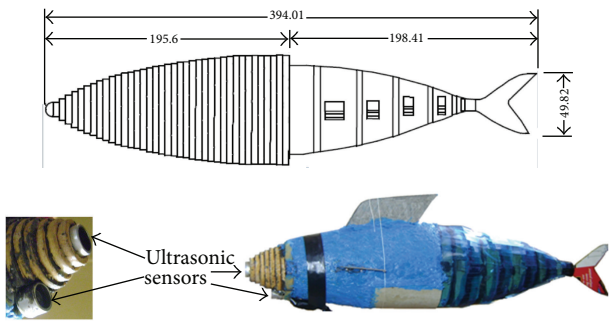

Figure 1: The biomimetic robotic fish that was being investigated. The receiver is at the tip and the transmitter is at the bottom.

Also without side lobe transmission attenuation, there will be multiple-object detection that is not directly ahead of the sonar transmitter.

In some situations, the problems associated with sonar navigation or object detection are augmented for by other sensing methods, for example, Asakawa et al. [17] AUV had the underwater cable to be located and carried a signature in the form of 16–25 Hz electric current which enabled it to automatically locate it. Another augmentation is in the form of bump switch to assist in navigating very tight environment where sonar ranging will be too close or ineffective [18]. Also Lygouras et al. [19] used terrain structure to augment the sonar navigation processes which fall into the categories referred to as baseline navigation systems [20, 21].

2. The Motivation

Our team built a biomimetic robotic fish named BlueMac (Figure 1)—a 1 : 1 scale model of Mackerel fish to investigate the use of rubber for building planar hyperredundant robot joint [18]. The robot is meant to swim in a low pressure head environment such as shallow lake, pond, or stream where water flow is not very strong or turbulent. It was meant to use commercially available 40 kHz ultrasonic transmitter/receiver combination for its navigation among obstacle fields, but it failed to work in all the possible configurations we tried except out of water. The sensors were sealed against water with materials of various thicknesses such as polythene and oil-impregnated paper. In one of the experiments, low-density mineral oil (used for sewing machine lubrication) was used to fill the void in front of the sensors to improve contact with the water boundary. As a last attempt, the sensors (transmitter and receiver) were immersed in water without any insulation—based on the premises that water is a poor conductor compared to the metallic conductor the sensor uses—this still yielded no result. Our conclusion was that the transmitter must have been overloaded for the following reasons:

(1) The piezo crystal plates drive the medium they are in forward and backward at the applied frequency.

(2) This action is not a problem when the fluid it is interacting with is air, with average density of 1.184 kg/m^3 (25.9°C mean temperature).

(3) If the fluid is water, the density becomes approximately 1000 kg/m^3, which is 847-fold increment of mass of fluid to move when compared to air. This seems to be an overload for the small-aperture sonar sensor.

Exhaustive literature search gave no clue on how to solve this problem except that Jindong and Huosheng [22–24] seemed to have encountered such problem also. They created an ultrasonic-based model for their robotic fish but implemented it with infrared light sensor. There are attempts by some researchers to imitate fish lateral lines [25–28] but small-scale purely sonar-based underwater navigation by robots that are less than 0.5 m in length is unknown to the authors as of this writing and this has prompted us to do a thorough investigation about it at this scale.

3. Objectives of This Study

The goal of this study is to setup a simulation environment in ANSYS Multiphysics software to find out the mode shapes of audible range piezo crystal (PZT-5H) material (commonly used in 27 mm diameter commercial buzzer alarms) at its harmonics. We also aim at finding possible nodal shape within the audible range (0–22 kHz) which implies absence of compressive and tensile stress simultaneously on one surface of the piezoelectric biomorph plate. Furthermore, we aim to test the piezo plates at higher frequencies so as to find out their real responses.

4. Theoretical Background

A piezoelectric material will generate voltages when subjected to tension or compression. The voltage generated is proportional to the compressive or tension load which is mathematically represented as [29, 30]

$$\begin{aligned} \{S\} &= \left[s^E\right]\{T\} + \left[d_t\right]\{E\} \\ \{D\} &= [d]\{T\} + \left[\epsilon^T\right]\{E\}, \end{aligned} \tag{1}$$

where S is strain vector, T is the vector of stresses, D is the dielectric displacement vector, E is the electric field vector, S^E is the compliance matrix evaluated at constant electric field, d is the piezoelectric strain coefficients, d_t is the mode of operation (compressive or transverse mode), and ϵ^T is

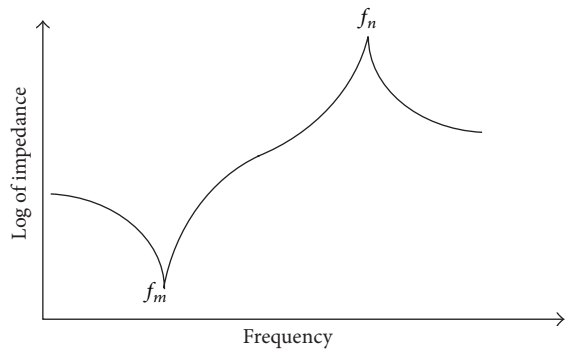

Figure 2: The signal response of matched piezo crystal transmitter and receiver.

Figure 3: Watch buzzer crystal plates.

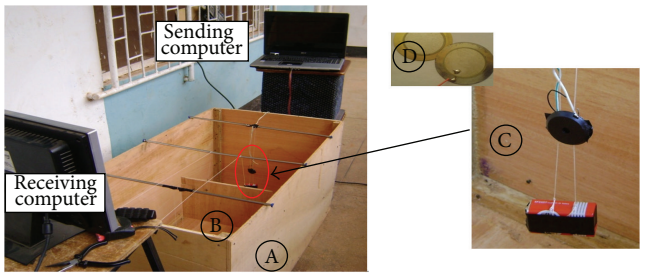

Figure 4: The preliminary experimental setup. (A) is the wooden box tank (without water), (B) is the obstacle place, (C) is the enlarge view of the piezo crystal plates, and (D) with sinker.

the dielectric constant matrix evaluated at constant stress. These equations (called "coupled" equations) reduce to the well-known stress-strain relationship at zero electric field and the electric field and charge displacement relationship at zero stress. The poling direction is a plane perpendicular to the flat side of the piezoelectric plate.

Furthermore, when piezoelectric plates are subjected to cyclic loading electrically, the usual response is shown in Figure 2. As the cyclic input frequency increases, there exist values at which the piezo element exhibits low impedance (f_m) and resonate. As the cyclic load frequency increases, there exists also another frequency at which it has the highest impedance, referred to as antiresonance frequency (f_n). Piezo plates working in pair (one acting as a transmitter and the other as a receiver) are selected in such a manner that the transmitter resonant frequency coincides with the receiver antiresonance frequency.

5. Methodology

5.1. Preliminary Experimentation. A preliminary experiment was performed to find out the potential of using ordinary buzzer plate (Figure 3) for underwater navigation using the idea from [31]. The following list of material was used for this preliminary experiment:

(1) two Intel-based computer systems (Dell Latitude cpτ with Celeron 500 MHz and and IBM clone with Intel Pentium 4),

(2) spectraPlus 5 software (shareware) installed on the two computers,

(3) two 2 cm back plate old wrist watch buzzer,

(4) water tank 50 cm × 50 cm × 121 cm (width, height, length),

(5) plain cable (wire),

(6) obstacles—plywood (6.35 mm) flat PVC (~1.5 mm), iron sheet (~1 mm) and asbestos (~2 mm) thicknesses.

The SpectraPlus 5 software in the Dell Latitude laptop (Figure 4) acts as the precision transmitter, while the one in the other computer acts as a receiver and spectrum analyzer. The line-out and line-in ports of the computers were used to drive the piezo plates in the sending and receiving computers, respectively. The experiment was started by first finding out the frequency between 0 Hz to 22 kHz that will give peak response (at the receiver end). The frequency that gave peak output was found to be 4.5 kHz. This value was therefore used for the underwater transmission preliminary tests. The tests involve spacing the plates at distances of 30 cm and 60 cm in the air and water while obstacles were placed in between them at equal distances from both the receiver and transmitter plates.

5.2. Mode Shape Simulation Processes and the Harmonic Analysis. The mode shape refers to the bending or contour pattern of the piezo crystal plates at its harmonics. ANSYS

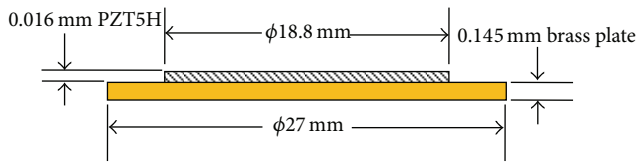

Figure 5: Dimension of plate.

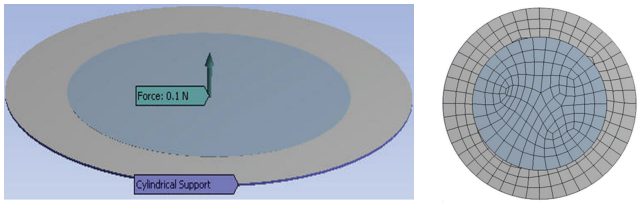

Figure 6: The simulation environment constraints and the mesh pattern as used for the simulation.

10 Multiphysics software was used for all the simulations while Autodesk Inventor software was used for all the geometrical drawings. The harmonic analysis was performed from 0 Hz to 22 kHz and then from 20 kHz to 100 kHz using harmonic tools built into ANSYS 10 Multiphysics. The analyses performed are (a) directional deformation, (b) frequency response, and (c) phase response; all were at a plane perpendicular to the piezo crystal plate surface.

5.3. The Simulation Environment. Frequency finder tool built into ANSYS Multiphysics was used with shape-optimized meshing. The simulation was performed for the 0 Hz to 22 kHz range. A dummy input load of 0.1 N (normal to the plate assembly) was used. For the higher frequencies 40, 60, 80, and 100 kHz, the surface deformation was estimated at these frequencies using harmonic tool directional deformation command. The dimension of the piezo crystal plate assembly used is shown in Figure 5. The constraints applied are shown in Figure 6 with the optimized mesh pattern. In Figure 6, a 0.1 N dummy load is shown acting perpendicularly to the piezo plate surface; this is to ensure a degree of deformation. Choosing a higher value will result in greater deformation which is equivalent to increasing the voltage at the piezo plate terminals. Higher or lower dummy load has no effect on the plate frequency response.

5.4. Experimental Verification of Transmission at 4.5, 10, 20, 40, 60, 80, and 100 kHz Frequencies. An experiment was setup to find out the wave pattern as the frequency increases using setup similar to Figure 4. The idea here is to find out if the piezo plate arrangement can follow the input signal and what the distortion in the output signal will be as the frequency increases.

This experiment uses Microchip PIC18F4520 microcontroller to generate a precise 5 V p-p square wave signal at selected frequencies of 4.5, 10, 20, 40, 60, 80, and 100 kHz. The output of the microcontroller was used to drive one of the piezo crystal plates while the other plate acts as the receiver. Both plates were connected to an oscilloscope for monitoring. The plates are 50 mm apart and immersed inside water at room temperature of 28°C.

Square wave signal was used as the input signal. The rise and fall (of the signal edge) approximate an impulsive loading. If the piezo plate assembly is approximated by a linearly damped mass-spring body (voigt body), the impulsive input implies that its response will give its dynamic characteristic [32, 33]. For linear time-invariant system (for which is an approximation in this scenario), the impulsive response is given by

$$C(s) = G(s)\,R(s) = G(s), \tag{2}$$

where $L\delta(t) = 1 = R(s)$ and transfer function $= C(s)/R(s) = G(s)$; therefore $c(t) = L^{-1}G(s) = g(t)$ and using convolution integral,

$$c(t) = \int_0^t g(t-\tau)\,r(\tau)\,d\tau, \tag{3}$$

the system's response can be found to any input [32, 33]. Summarily, driving the sample with a square wave signal allows us to have an idea about its realistic response which will be a function of its nature.

6. Results Obtained

6.1. The Result of the Preliminary Experiment. The results obtained in the preliminary experiment are shown in Figure 7 and Table 2. Table 2 also shows the relative absorption value which we hereby define as the difference in magnitudes in peak response in air and water with the same piezo plate spacing, specifically as illustrated in (4).

$$|R_{\text{water}}| - |R_{\text{air}}| \quad \text{at equal spacing.} \tag{4}$$

6.2. The Result of Mode Shape Simulation Processes and the Harmonic Analysis. The 15 harmonics existing between 0 Hz and 22 kHz as simulated by ANSYS 10 Multiphysics are shown in Figure 8. Each pair of adjacent pictures shows plan view and side or isometric view of the mode shape at the harmonic frequencies indicated below them. When the simulation input frequencies were set at 40, 60, 80, and 100 kHz, that is, above the audible range, the mode shapes were as shown in Figure 9 for each input frequency.

Furthermore, the frequency response curves for 0 to 22 kHz and 20 kHz to 100 kHz input ranges are plotted in

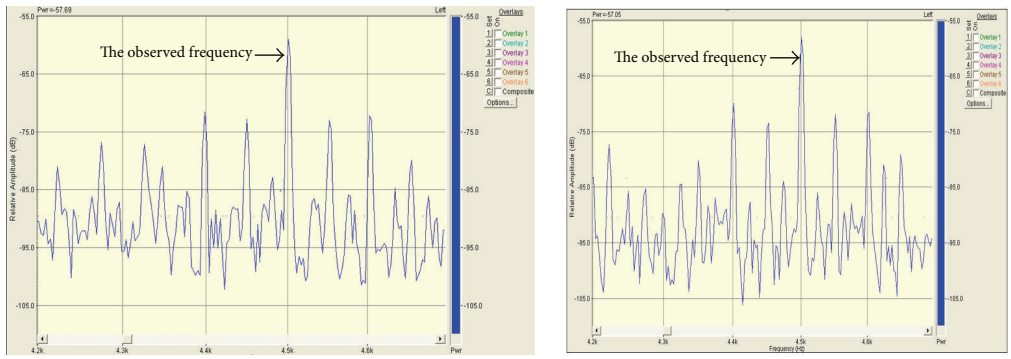

30 cm apart 60 cm apart

Figure 7: Spectrums obtained when transmitter and receiver were 30 and 60 cm apart in water and no object in between them.

Table 2: Summary of the peak response with and without obstacles in the air and water.

Material used	Relative amplitude (dB) in air at		Relative amplitude (dB) in water at		Relative absorption at	Relative absorption at
	30 cm	60 cm	30 cm	60 cm	30 cm	60 cm
No object	−71.29	−81.47	−11.13	−23.56	−60.16	−57.91
Plywood	−88.95	−90.68	−34.11	−32.63	−54.84	−58.05
Asbestos	−83.12	−88.22	−27.40	−30.94	−55.72	−57.28
PVC plastics	−78.95	−81.36	−24.76	−30.21	−54.19	−51.15
Iron sheet	−86.17	−89.12	−20.63	−23.33	−65.54	−65.79

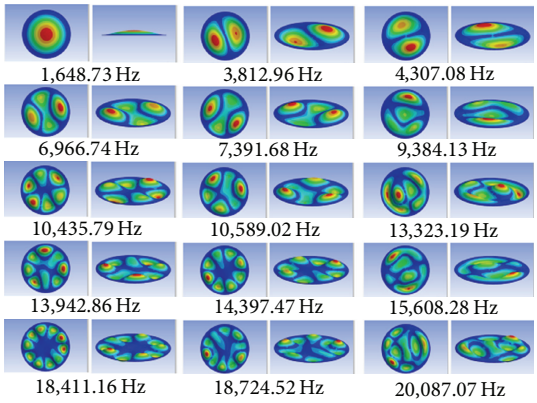

Figure 8: Mode shapes at various harmonics as indicated at the bottom of each pair of view.

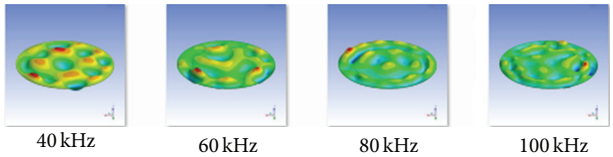

Figure 9: Mode shapes at fixed frequencies indicated.

Figures 10 and 11, respectively. The maximum and minimum deformation at axis perpendicular to the plate face is shown in Figure 12(a) along with the total displacement at each harmonic (Figure 12(b)). Table 3 is the maximum deformation for the indicated frequencies. The total displacement plot without the first natural frequency of 1648.73 Hz is shown in Figure 13. Phase response analysis for the frequency range of 100 to 20 kHz and 20 kHz to 100 kHz gave the plots of Figures 14 and 15, respectively. Figure 16 is the frequency response plot for 20 kHz to 100 kHz input frequency range. The inset in Figure 16 has frequency range of 52 kHz to 67 kHz.

6.3. Results of the Experimental Verification of Transmission at 4.5, 10, 20, 40, 60, 80, and 100 kHz Frequencies. The experimental verification at 4.5, 10, 20, 40, 60, 80, and 100 kHz frequencies is shown in Figure 17. The upper trace is the input signal and the lower trace is the output signal on a dual-trace oscilloscope.

7. Discussion of the Results

7.1. The Preliminary Experiment. The frequency of interest is 4.5 kHz (Figure 7), the other frequencies indicated are artifacts due to the use of unshielded cable (since this is a preliminary investigation). Also, from Table 2, the followings can be observed:

(1) The signal strength drops with distance between the transmitter plate and receiver plate (while in the air and water medium).

(2) With obstacles in between the plates, the plywood influence on the signal strength is opposite to that of

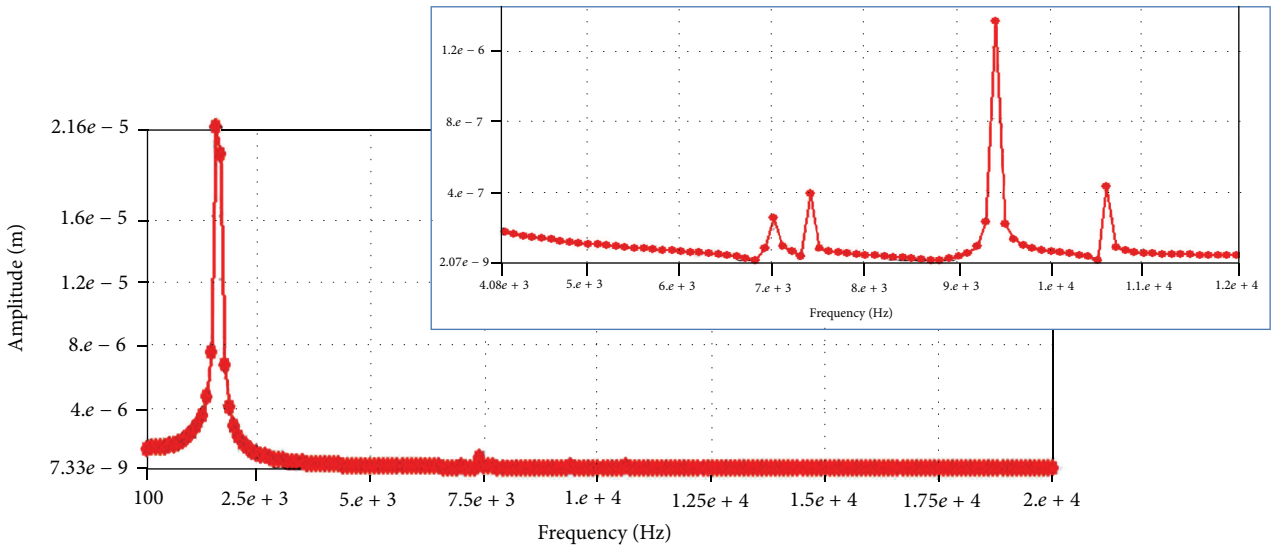

Figure 10: Frequency response plot for 100 Hz–20 kHz range. The inset is from 4.08 kHz to 12 kHz.

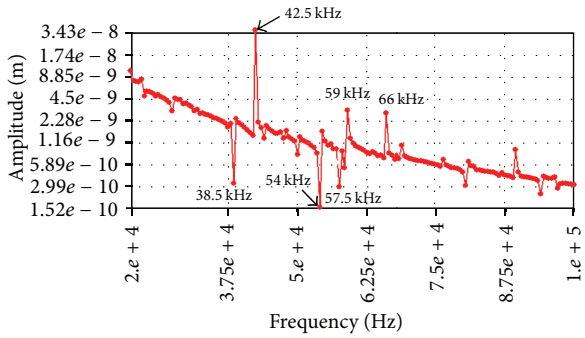

Figure 11: Frequency response plot for 20 kHz–100 kHz showing a general drop with spikes and deeps corresponding to resonance and antiresonance, respectively.

the others when the experiment was conducted inside water—the signal strength is less affected by it.

(3) The relative absorption at 60 cm is less than that at 30 cm (as defined in (4)) generally except for the plywood obstacle.

(4) Generally, the signal strength for the experiment inside water is always higher than that conducted in the air by approximately 4 times. We attribute this to better coupling of solid-liquid interfaces than solid-air (gas) interface.

7.2. Mode Shape Simulation Processes and the Harmonic Analysis. There are 15 harmonics (Figure 8) between 0 Hz and 22 kHz as simulated by ANSYS 10 Multiphysics. Only the first harmonic exhibits nodal shape while some of the other harmonics are inverse of the subsequent harmonic frequency. The frequencies used in Figure 9 were selected to be 20 kHz apart and are not harmonics (they were checked using ANSYS multiphysics). None of the simulation in Figure 9 has nodal shape; they all seems to have the same area of crests and valleys.

Table 3: Maximum deformation for indicated frequencies.

	Frequency (Hz)	Maximum surface deformation (m)	Remark
(1)	1,648.73	5.53$E-02$	
(2)	3,812.96	3.15$E-05$	
(3)	4,307.08	4.53$E-05$	
(4)	6,966.74	2.35$E-03$	
(5)	7,391.68	1.85$E-03$	
(6)	9,384.13	7.32$E-03$	
(7)	10,435.79	4.89$E-05$	
(8)	10,589.02	3.52$E-03$	The first 15 harmonics occurring between 0–22 kHz
(9)	13,323.19	6.07$E-05$	
(10)	13,942.86	8.64$E-05$	
(11)	14,397.47	4.24$E-06$	
(12)	15,608.28	2.31$E-06$	
(13)	18,411.16	2.12$E-05$	
(14)	18,724.52	3.14$E-05$	
(15)	20,087.07	4.71$E-04$	
f_1	40,000.00	1.33$E-08$	Higher frequencies
f_2	60,000.00	1.23$E-08$	
f_3	80,000.00	9.11$E-09$	
f_4	100,000.00	2.60$E-09$	

The plots of Figure 11 further show that there are lots of resonance frequencies (peeks) and antiresonance frequencies

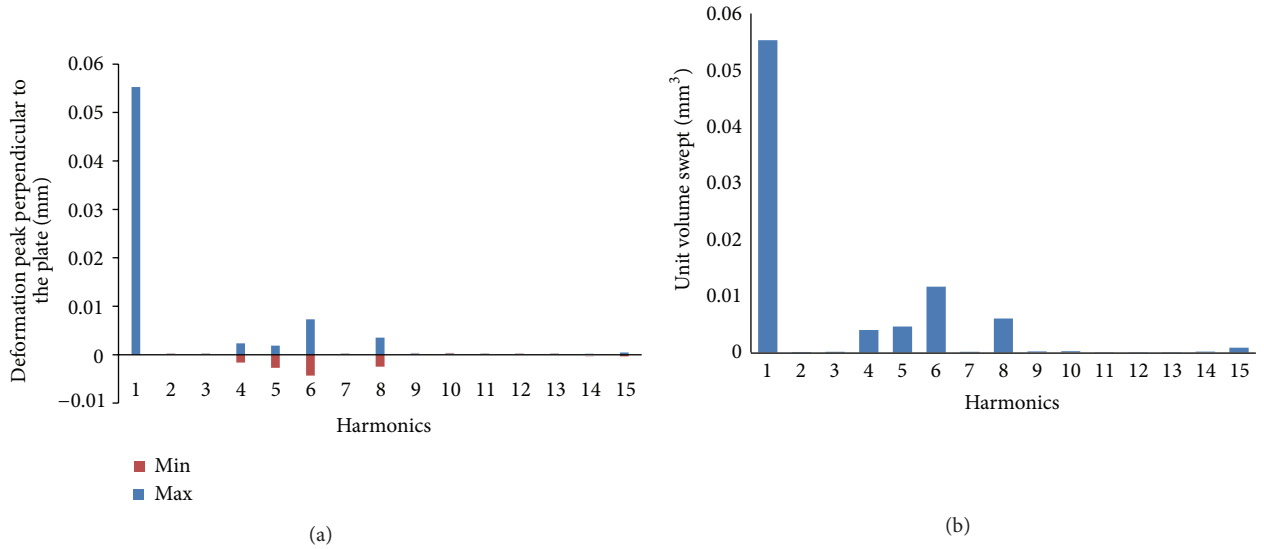

Figure 12: Plot of maximum and minimum deformation in Z direction (perpendicular to the plate surface) (a) and total displacement by the plate at various harmonics (b).

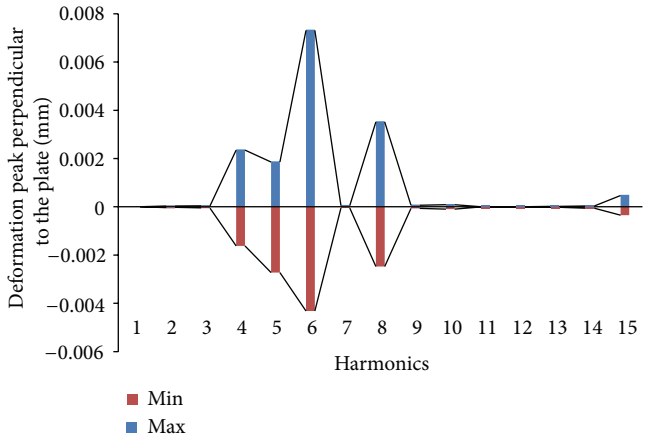

Figure 13: Plot of maximum and minimum deformation in Z direction, the first harmonics is ignored in this plot.

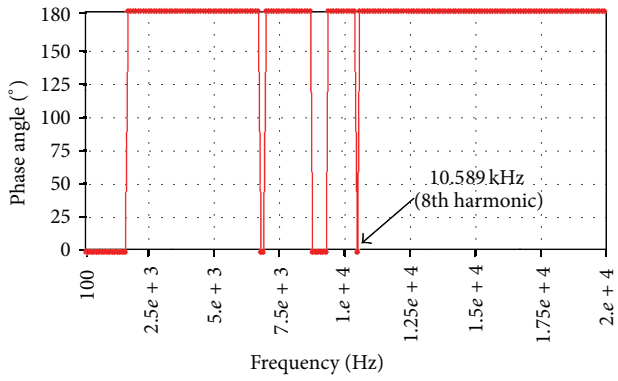

Figure 14: Phase response plots for 100 Hz–20 kHz range.

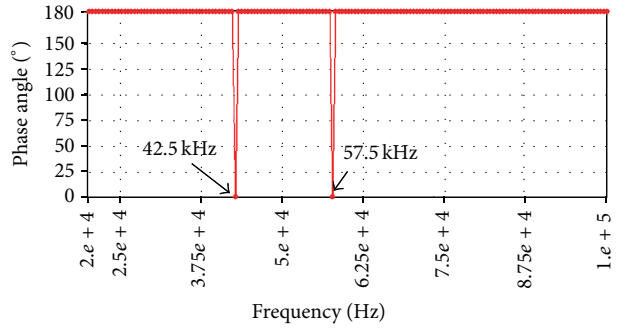

Figure 15: Phase response plots for 20 kHz–100 kHz range.

(deeps); however, the 0–22 kHz (audio range) of Figure 10 does not exhibit such pattern. Also the frequency response generally drops as the frequency increases for the ranges (0–22 kHz and 20–100 kHz) combined.

The maximum and minimum deformation at axis perpendicular to the plate face is shown in Figures 12 and 13. A closer study of Figures 8, 12, and 13 shows that the 2nd and 3rd natural frequencies have crests and valleys that occupy about the same area. The same applies to the 7^{th} and 9th–14th harmonics. The 1st, 4th, 5th, 6th, 8th, and 15th harmonics have unequal crest and valley areas. This cancels out each other displacement. This is more glaring with the 1st harmonic that has zero valley areas. The 40, 60, 80, and 100 kHz displacements are much lower in comparison to those of the natural frequencies occurring in the 0–22 kHz range as shown in Table 3. The implication is that much energy must be used to increase the piezo plate displacements at these higher frequencies.

One lesson that can be learned from this behavior is that the harmonics 1, 4, 5, 6, 8, and 15 are to be invested in as they sweep more volume of the media than other

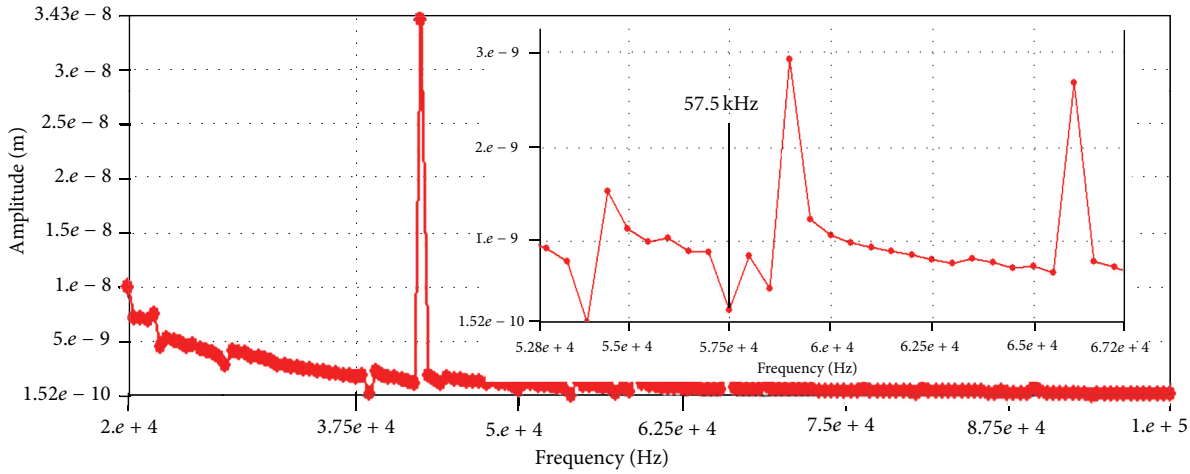

Figure 16: Frequency response plot for 20 kHz–100 kHz range. The inset is from 52 kHz to 67 kHz.

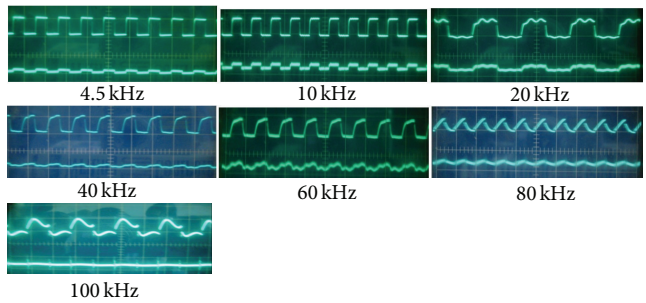

Figure 17: The transmission and reception degrade in quality as the square wave input frequency was increased. For each output, the top trace is the input and the lower trace is the response of the receiving piezo plate.

harmonics. For practical purposes and where a bit audible output is not disturbing, the 1st harmonic is the most ideal, but where audibility is undesired, higher harmonics such as the 15th harmonic should be used. We are not affirming that frequencies above 22 kHz will not work but, as expected, more energy will have to go in to drive the plates as the output will be very low.

A phase response analysis for the harmonics, Figure 14, shows that lower frequencies up to 1,648.73 Hz (first harmonic) and then at 6,966.74 Hz (fourth harmonic) and 9,384.13 Hz (sixth harmonic) are in phase (0°). At high frequencies, Figure 15, the frequencies 42.5 kHz and 57.5 kHz are also in phase with the input, but the 57.5 kHz is an antiresonance (a deep-lowered amplitude) as shown in the inset of Figure 16. The deep is a trap to be watched for when optimizing the transmitter output.

7.3. The Experimental Verification of Transmission at 4.5, 10, 20, 40, 60, 80, and 100 kHz Frequencies. At higher frequencies, the receiver output drops and are derivative (spikes) of the square wave input especially for the 100 kHz test frequency. Also the transmitter output depreciates from a perfect square wave as frequency increases with discontinuity in the oscilloscope plot. It is also noticeable from Figure 17 that this piezo plate assembly is able to follow the input better at the test signals of 40 kHz and 60 kHz compared to the test signals of 80 kHz and 100 kHz.

8. Conclusion

The immediate implication of this work is that we can use ordinary buzzer piezo plate for underwater navigation (at least for a short range of about 2 m or less, we used maximum of 0.6 m in this work) by transmitting at a selected higher frequency. In selecting a higher frequency above audio, we can take the advantage of the knowledge that 40 kHz to 60 kHz test input signal can work as earlier explained and combine that knowledge with the fact that there is a harmonic nearby, that is, 42.5 kHz which we can tune into and an antiresonance frequency nearby such as 57.5 kHz which will give a much lowered output and should not be used.

As shown in this paper, this common buzzer worked well as an underwater transmitter-cum-receiver at audible range of 0–22 kHz which implies that a short range-low-power underwater navigation device can be realized using

buzzer plates. A carefully selected resonance frequency can be used with a matching receiver piezo plate that is tuned to its resonant frequency for reflective sonar sensing.

For the robotic fish we developed, short-range communication is desired. For example, when investigating cluttered environment such as underwater crevices, short range and reliable ultrasonic sensor will work well and especially if the water is mucky.

Disclosure

The authors want to recommend that a realistic sonar-based navigation, object detection, and avoidance using this type of piezo plate described in this work should be developed and tested using higher frequencies (above 22 kHz) that are resonance. Though not discussed in this work, the issue of side lobe transmission and wave guide or signal concentrator needs to be investigated for low-power small-scale underwater robots based on the buzzer piezo crystal plate.

References

[1] R. M. Eustice, H. Singh, and L. L. Whitcomb, "Synchronous-clock, one-way-travel-time acoustic navigation for underwater vehicles," *Journal of Field Robotics*, vol. 28, no. 1, pp. 121–136, 2011.

[2] M. Kumagai, T. Ura, Y. Kuroda, and R. Walker, "A new autonomous underwater vehicle designed for lake environment monitoring," *Advanced Robotics*, vol. 16, no. 1, pp. 17–26, 2002.

[3] G. Grenon, P. E. An, S. M. Smith, and A. J. Healey, "Enhancement of the inertial navigation system for the Morpheus autonomous underwater vehicles," *IEEE Journal of Oceanic Engineering*, vol. 26, no. 4, pp. 548–560, 2001.

[4] X. Yun, E. R. Bachmann, S. Arslan, K. Akyol, and R. B. McGhee, "An inertial navigation system for small autonomous underwater vehicles," *Advanced Robotics*, vol. 15, no. 5, pp. 521–532, 2001.

[5] H. Bo, Z. Hongjin, L. Chao, Z. Shujing, L. Yan, and Y. Tianhong, "Autonomous navigation for autonomous underwater vehicles based on information filters and active sensing," *Sensors*, vol. 11, pp. 10958–10980, 2011.

[6] E. Durá, J. Bell, and D. Lane, "Reconstruction of textured seafloors from side-scan sonar images," *IEE Proceedings*, vol. 151, no. 2, pp. 114–126, 2004.

[7] C. G. Capus, A. C. Banks, E. Coiras, I. Tena Ruiz, C. J. Smith, and Y. R. Petillot, "Data correction for visualisation and classification of sidescan SONAR imagery," *IET Radar, Sonar and Navigation*, vol. 2, no. 3, pp. 155–169, 2008.

[8] A. Negre, C. Pradalier, and M. Dunbabin, "Robust vision-based underwater homing using self-similar landmarks," *Journal of Field Robotics*, vol. 25, no. 6-7, pp. 360–377, 2008.

[9] T. Kodama, K. Nakahira, Y. Kanaya, and T. Yoshikawa, "Application of digital polarity correlators in a sonar ranging system," *Electronics and Communications in Japan*, vol. 91, no. 4, pp. 20–26, 2008.

[10] T. C. Austin, "The application of spread spectrum signaling techniques to underwater acoustic navigation," in *Proceedings of the IEEE Symposium on Autonomous Underwater Vehicle Technology*, pp. 443–449, Boston, Mass, USA, July 1994.

[11] K. Vickery, "Acoustic positioning systems—a practical overview of current systems," in *Proceedings of the IEEE Symposium on Autonomous Underwater Vehicle Technology*, pp. 5–17, Cambridge, Mass, USA, August 1998.

[12] T. C. Austin and R. Stokey, "Relative acoustic tracking," *Sea Technology*, vol. 39, no. 3, pp. 21–27, 1998.

[13] S. M. Smith and D. Kronen, "Experimental results of an inexpensive short baseline acoustic positioning system for AUV navigation," in *Proceedings of the Oceans. MTS/IEEE Conference*, pp. 714–720, Boca Raton, Fla, USA, October 1997.

[14] B. Pierce, "Protecting Whales from Dangerous Sonar," 2008, http://www.nrdc.org/wildlife/marine/sonar.asp.

[15] L. J. Jennifer, "Sonar ban sounded good. A skeptical analysis," *Skeptic*, vol. 10, no. 4, pp. 14–15, 2004.

[16] T. G. Leighton, "From seas to surgeries, from babbling brooks to baby scans: the acoustics of gas bubbles in liquids," *International Journal of Modern Physics B*, vol. 18, no. 25, pp. 3267–3314, 2004.

[17] K. Asakawa, J. Kojima, Y. Kato et al., "Design concept and experimental results of the autonomous underwater vehicle AQUA EXPLORER 2 for the inspection of underwater cables," *Advanced Robotics*, vol. 16, no. 1, pp. 27–42, 2002.

[18] M. O. Afolayan, D. S. Yawas, C. O. Folayan, and S. Y. Aku, "Mechanical description of a hyper-redundant robot joint mechanism used for a design of a biomimetic robotic fish," *Journal of Robotics*, vol. 2012, Article ID 826364, 16 pages, 2012.

[19] J. Lygouras, V. Kodogiannis, T. Pachidis, and P. Liatsis, "Terrain-based navigation for underwater vehicles using an ultrasonic scanning system," *Advanced Robotics*, vol. 22, no. 11, pp. 1181–1205, 2008.

[20] J. N. Lygouras, C. M. Dimitriadis, M. C. Tsortanidis, G. C. Bakos, and P. G. Tsalides, "Digital ultrasonic scanning system for positioning underwater remotely operated vehicles," *International Journal of Electronics*, vol. 76, no. 3, pp. 541–550, 1994.

[21] J. N. Lygouras, K. A. Lalakos, and P. G. Tsalides, "THETIS: an underwater remotely operated vehicle for water pollution measurements," *Microprocessors and Microsystems*, vol. 22, no. 5, pp. 227–237, 1998.

[22] L. Jindong and H. Huosheng, "Building a simulation environment for optimising control Parameters of an Autonomous Robotic Fish," in *Proceedings of the 9th Chinese Automation & Computing Society Conference in the UK, Luton, England*, September 2003.

[23] J. Liu and H. Hu, "Building a 3D simulator for autonomous navigation of robotic fishes," in *Proceedings of the IEEE/RSJ International Conference on Intelligent Robots and Systems (IROS '04)*, pp. 613–618, Sendai, Japan, October 2004.

[24] J. Liu and O. Hu, "A methodology of modelling fish-like swim patterns for robotic fish," in *Proceedings of the IEEE International Conference on Mechatronics and Automation (ICMA '07)*, pp. 1316–1321, Harbin, China, August 2007.

[25] F. Zhifang, C. Jack, Z. Jun, B. David, and L. Chang, "Design and fabrication of artificial lateral line flow sensors," *Journal of Micromechanics and Microengineering*, vol. 12, pp. 655–661, 2002.

[26] Y. Yang, J. Chen, J. Engel et al., "Distant touch hydrodynamic imaging with an artificial lateral line," *Proceedings of the National Academy of Sciences of the United States of America*, vol. 103, no. 50, pp. 18891–18895, 2006.

[27] J. C. Liao, "The role of the lateral line and vision on body kinematics and hydrodynamic preference of rainbow trout in turbulent flow," *Journal of Experimental Biology*, vol. 209, part 20, pp. 4077–4090, 2006.

[28] Y. Yang, N. Nguyen, N. Chen et al., "Artificial lateral line with biomimetic neuromasts to emulate fish sensing," *Bioinspiration and Biomimetics*, vol. 5, no. 1, Article ID 016001, 2010.

[29] J. Sirohi and I. Chopra, "Fundamental understanding of piezoelectric strain sensors," *Journal of Intelligent Material Systems and Structures*, vol. 11, no. 4, pp. 246–257, 2000.

[30] IEEE Standard on Piezoelectricity, "Standard Committee of the IEEE Ultrasonics, Ferroelectrics, and Frequency Control Society," ANSI/IEEE Std 176-1987.

[31] M. O. Afolayan, "Potential of watch buzzer as underwater navigation device in shallow water streams," *Research Journal of Applied Sciences, Engineering and Technology*, vol. 2, no. 5, pp. 436–446, 2010.

[32] O. Katsuihiko, *Modern Control Engineering*, Pearson Education, 4th edition, 2005.

[33] I. J. Nagrath and M. Gopal, *Control Systems Engineering*, Publisher New Age International Publishers, 4th edition, 2005.